BIOCHEMISTRY
including biophysical chemistry & molecular biology

Article

pubs.acs.org/biochemistry

Multivalent Binding and Facilitated Diffusion Account for the Formation of the Grb2−Sos1 Signaling Complex in a Cooperative Manner

Caleb B. McDonald, Jordan E. Balke, Vikas Bhat, David C. Mikles, Brian J. Deegan, Kenneth L. Seldeen, and Amjad Farooq*

Department of Biochemistry and Molecular Biology and USylvester Braman Family Breast Cancer Institute, Leonard Miller School of Medicine, University of Miami, Miami, Florida 33136, United States

ABSTRACT: Despite its key role in driving cellular growth and proliferation through receptor tyrosine kinase (RTK) signaling, the Grb2−Sos1 macromolecular interaction remains poorly understood in mechanistic terms. Herein, using an array of biophysical methods, we provide evidence that although the Grb2 adaptor can potentially bind to all four PXψPXR motifs (designated herein S1−S4) located within the Sos1 guanine nucleotide exchange factor, the formation of the Grb2−Sos1 signaling complex occurs with a 2:1 stoichiometry. Strikingly, such bivalent binding appears to be driven by the association of the Grb2 homodimer to only two of four potential PXψPXR motifs within Sos1 at any one time. Of particular interest is the observation that of a possible six pairwise combinations in which S1−S4 motifs may act in concert for the docking of the Grb2 homodimer through bivalent binding, only S1 and S3, S1 and S4, S2 and S4, and S3 and S4 do so, while pairwise combinations of sites S1 and S2 and sites S2 and S3 appear to afford only monovalent binding. This salient observation implicates the role of local physical constraints in fine-tuning the conformational heterogeneity of the Grb2−Sos1 signaling complex. Importantly, the presence of multiple binding sites within Sos1 appears to provide a physical route for Grb2 to hop in a flip-flop manner from one site to the next through facilitated diffusion, and such rapid exchange forms the basis of positive cooperativity driving the bivalent binding of Grb2 to Sos1 with high affinity. Collectively, our study sheds new light on the assembly of a key macromolecular signaling complex central to cellular machinery in health and disease.

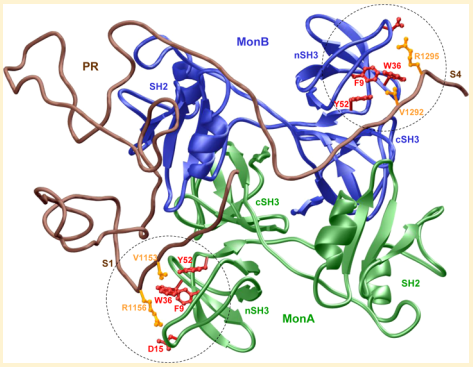

The Grb2−Sos1 interaction plays a central role in relaying external signals from receptor tyrosine kinases (RTKs) at the cell surface to downstream effectors and regulators such as Ras and Akt within the cytosol.[1−4] Comprised of the ubiquitous nSH3-SH2-cSH3 signaling module, where nSH3 and cSH3 are the N-terminal and C-terminal SH3 domains, respectively, flanking the central SH2 domain, Grb2 recognizes activated RTKs by virtue of the ability of its SH2 domain to bind to tyrosine-phosphorylated (pY) sequences in the context of the pYXN motif located within the cytoplasmic tails of a diverse array of receptors, including EGF and PDGF receptors.[5−7] Upon binding to RTKs, the SH3 domains of Grb2 present an opportunity for a wide spectrum of proline-rich proteins to be recruited to the inner membrane surface, the site of initiation of a plethora of signaling cascades.[3,8−15] Among them, the Sos1 guanine nucleotide exchange factor and the Gab1 docker are by far the best characterized downstream partners of Grb2.[8−10,16,17] Upon recruitment to the inner membrane surface, Sos1 facilitates GDP−GTP exchange within the membrane-bound Ras GTPase and thereby switches on a key signaling circuit that involves the activation of the MAP kinase cascade central to cellular growth and proliferation.[18,19] In contrast, the recruitment of Gab1 to the inner membrane surface provides docking platforms for the Shp2 tyrosine phosphatase and the PI3K kinase, which account for further amplification of Ras activity, as sustained activation of Ras requires both Sos1-dependent and Gab1-dependent pathways,[20−23] and the activation of Akt serine-threonine kinase, which plays a pivotal role in cell growth and survival,[24] respectively.

How exactly does Grb2 recruit Sos1 to the inner membrane surface? Although seminal work implicated the role of both SH3 domains of Grb2 in the recruitment of Sos1 to the inner membrane surface,[3,8,17] recent studies have shown that only the nSH3 domain binds to Sos1 in an allosteric manner such that the cSH3 domain is freed up for binding to Gab1 to generate the Sos1−Grb2−Gab1 ternary signaling complex in a noncompetitive fashion.[25,26] It is important to note that Sos1 contains four distinct sites within its proline-rich (PR) domain for binding to the nSH3 domain of Grb2 (Figure 1). These sites, designated herein S1−S4, share the PXψPXR consensus motif, where X is any residue and ψ is valine, leucine, or isoleucine. On the basis of structural studies of the nSH3 domain of Grb2 in complex with peptides containing the PXψPXR motif in Sos1,[27−31] the nSH3 domain displays a characteristic β-barrel fold harboring a hydrophobic cleft on one face of the

Received: January 12, 2012
Revised: February 20, 2012
Published: February 24, 2012

   dx.doi.org/10.1021/bi3000534 | *Biochemistry* 2012, 51, 2122−2135

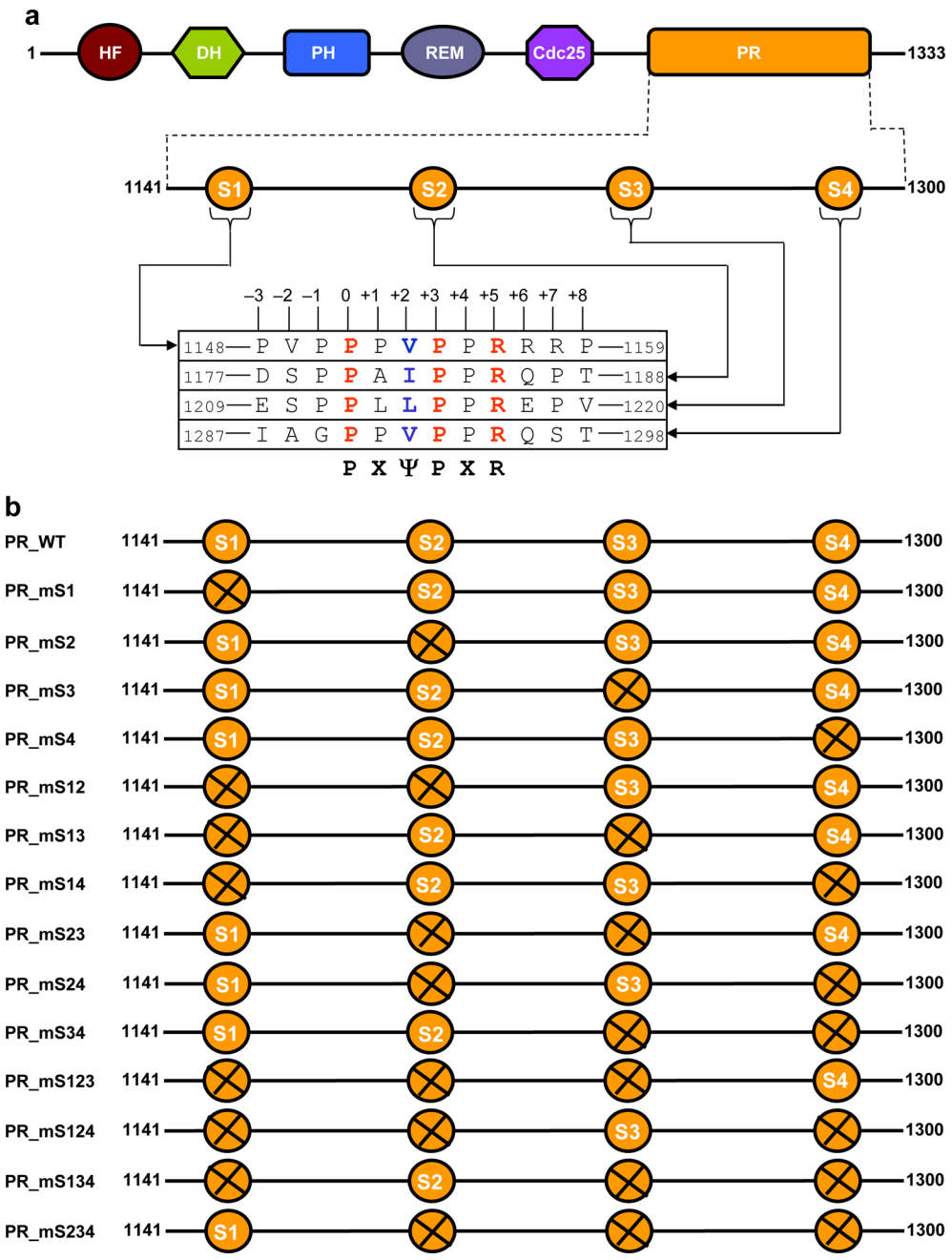

Figure 1. Domain organization of Sos1 and the maps of various constructs of its proline-rich (PR) domain. (a) The PR domain of Sos1 lies at the extreme C-terminal end and contains four distinct sites, herein designated S1−S4, characterized by the presence of the PXψPXR consensus motif. The complete sequences of these four sites are shown. The position of various residues relative to the first proline within the PXψPXR motif, which is designated zero, is also indicated. Other domains within Sos1 are HF (histone fold), DH (Dbl homology), PH (pleckstrin homology), REM (Ras exchange motif), and Cdc25. (b) Maps of wild-type (WT) and various mutant constructs of the PR domain of Sos1 used in this study. The wild-type PR construct (PR_WT) contains all four S1−S4 motifs. In the single-mutant PR constructs (PR_mS1, PR_mS2, PR_mS3, and PR_mS4), one of the four S1−S4 motifs is disrupted individually with the mutated site indicated by the prefix m. In contrast, the double-mutant PR constructs (PR_mS12, PR_mS13, PR_mS14, PR_mS23, PR_mS24, and PR_mS34) contain pairwise disruptions of all possible combinations of motifs S1−S4. Finally, the triple-mutant PR constructs (PR_mS123, PR_mS124, PR_mS134, and PR_mS234) were designed to disrupt all but one of the S1−S4 motifs. Note that the disruption of each of the four S1−S4 motifs, as indicated by a saltire (X), was achieved through alanine substitution of ψ and arginine residues within the corresponding PXψPXR consensus sequence, the integrity of which is required for their binding to the nSH3 domain of Grb2. The numerals at the ends of each construct indicate the amino acid sequence number within human Sos1.

domain for accommodating the incoming peptide. While the β-barrel is comprised of a pair of nearly orthogonal β-sheets, with each β-sheet containing three antiparallel β-strands, the peptide adopts a relatively open left-handed polyproline type II (PPII) helical conformation upon binding. Although our previous studies have shown that the isolated nSH3 domain of Grb2 can potentially bind to peptides derived from all four S1−S4 motifs in a physiologically relevant manner,[26,32,33] the precise mechanism of the assembly of the Grb2−Sos1 signaling complex remains hitherto poorly understood. In light of the knowledge that Grb2 exists in a dimer−monomer equilibrium in solution,[34] it is tempting to postulate that Grb2 could bind to

dx.doi.org/10.1021/bi3000534 | *Biochemistry* 2012, 51, 2122−2135

Sos1 in a multivalent manner to generate higher-order Grb2−Sos1 multimers rather than a simple binary complex.

In an effort to further elucidate the mechanism underlying the assembly of the Grb2−Sos1 signaling complex, we conceived this study. Herein, using an array of biophysical methods, we provide evidence that although the Grb2 adaptor can potentially bind to all four PXψPXR motifs, designated herein S1−S4, located within the Sos1 guanine nucleotide exchange factor, the formation of the Grb2−Sos1 signaling complex occurs with a 2:1 stoichiometry. Strikingly, such bivalent binding appears to be driven by the association of the Grb2 homodimer with only two of four potential PXψPXR motifs within Sos1 at any one time. Of particular interest is the observation that of a possible six pairwise combinations in which S1−S4 motifs may act in concert for the docking of the Grb2 homodimer through bivalent binding, only S1 and S3, S1 and S4, S2 and S4, and S3 and S4 do so, while pairwise combinations of sites S1 and S2 and sites S2 and S3 appear to afford only monovalent binding. This salient observation implicates the role of local physical constraints in fine-tuning the conformational heterogeneity of the Grb2−Sos1 signaling complex. Importantly, the presence of multiple binding sites within Sos1 appears to provide a physical route for Grb2 to hop in a flip-flop manner from one site to the next through facilitated diffusion, and such rapid exchange forms the basis of positive cooperativity driving the bivalent binding of Grb2 to Sos1 with high affinity. Collectively, our study sheds new light on the assembly of a key macromolecular signaling complex central to cellular machinery in health and disease.

MATERIALS AND METHODS

Sample Preparation. Full-length human Grb2 (residues 1−217) and the wild-type and various mutant constructs of the PR domain of human Sos1 (residues 1141−1300) were cloned into pET30 bacterial expression vectors with an N-terminal His tag using Novagen LIC technology. Notably, the mutant constructs of the PR domain of Sos1 were generated through alanine substitution of consensus ψ and arginine residues, located within the corresponding PXψPXR motifs, through de novo cDNA synthesis courtesy of GenScript Corp. (Figure 1). All recombinant constructs were expressed in the *Escherichia coli* BL21 Star(DE3) bacterial strain (Invitrogen) and purified on a Ni-NTA affinity column using standard procedures. Briefly, bacterial cells were grown at 20 °C in Terrific Broth to an optical density of >1 at 600 nm prior to induction with 0.5 mM isopropyl β-D-1-thiogalactopyranoside (IPTG). The bacterial culture was further grown overnight at 20 °C, and the cells were subsequently harvested and disrupted using a BeadBeater (Biospec). After separation of cell debris via high-speed centrifugation, the cell lysate was loaded onto a Ni-NTA column and washed extensively with 20 mM imidazole to remove nonspecific binding of bacterial proteins to the column. The recombinant proteins were subsequently eluted with 200 mM imidazole and dialyzed against an appropriate buffer to remove excess imidazole. Further treatment on a Hiload Superdex 200 size-exclusion chromatography (SEC) column coupled in-line with a GE Akta FPLC system led to purification of Grb2 and various constructs of the PR domain of Sos1 to apparent homogeneity as judged by sodium dodecyl sulfate−polyacrylamide gel electrophoresis analysis. Final yields were typically between 10 and 20 mg of protein of apparent homogeneity per liter of bacterial culture. Protein concentrations were determined by the fluorescence-based Quant-It assay (Invitrogen) and spectrophotometrically on the basis of extinction coefficients calculated for each recombinant construct using the online software ProtParam at ExPasy Server.[35] Results from both methods were in excellent agreement.

Analytical Light Scattering. Analytical light scattering (ALS) experiments were conducted on a Wyatt miniDAWN TREOS triple-angle static light scattering detector and Wyatt QELS dynamic light scattering detector coupled in-line with a Wyatt Optilab rEX differential refractive index detector and interfaced with a Hiload Superdex 200 size-exclusion chromatography (SEC) column under the control of a GE Akta FPLC system within a chromatography refrigerator at 10 °C. Protein samples of full-length Grb2 and various constructs of the PR domain of Sos1 were prepared in 50 mM Tris, 200 mM NaCl, 1 mM EDTA, and 5 mM β-mercaptoethanol (pH 8.0) and loaded onto the column at a flow rate of 1 mL/min, and the data were automatically acquired using ASTRA. The starting concentrations injected onto the column were typically between 40 and 50 μM for each protein construct. The angle and concentration dependence of static light scattering (SLS) intensity of each protein species resolved in the flow mode was measured by the Wyatt miniDAWN TREOS detector. The SLS data were analyzed according to the following built-in Zimm equation in ASTRA:[36,37]

$$Kc/R_\theta = (1/M + 2A_2c)\{1 + [16\pi^2(R_g)^2/3\lambda^2]\sin^2(\theta/2)\} \quad (1)$$

where R_θ is the excess Raleigh ratio due to protein in the solution as a function of protein concentration c (milligrams per milliliter) and scattering angle θ (42°, 90°, and 138°), M is the observed molar mass of each protein species, A_2 is the second virial coefficient, λ is the wavelength of laser light in solution (658 nm), R_g is the radius of gyration of the protein, and K is given by the following relationship:

$$K = [4\pi^2 n^2 (dn/dc)^2]/(N_A\lambda^4) \quad (2)$$

where n is the refractive index of the solvent, dn/dc is the refractive index increment of the protein in solution, and N_A is Avogadro's number (6.02×10^{23} mol^{-1}). At dilute protein concentrations ($c \rightarrow 0$), eq 1 reduces to

$$Kc/R_\theta = 1/M + [16\pi^2(R_g)^2/3M\lambda^2]\sin^2(\theta/2) \quad (3)$$

Thus, a plot of Kc/R_θ versus $\sin^2(\theta/2)$ yields a straight line with a slope of $(16\pi^2R_g^2)/(3M\lambda^2)$ and a y-intercept of $1/M$. Accordingly, the molar mass can be obtained in a global analysis from the y-intercept of linear fits of a range of Kc/R_θ versus $\sin^2(\theta/2)$ plots as a function of protein concentration along the elution profile of each protein species using SLS measurements at three scattering angles. Herein, the weight-average molar mass (M_w) and number-average molar mass (M_n) were calculated from the following relationships:

$$M_w = \sum (c_iM_i)/\sum c_i \quad (4)$$

$$M_n = \sum c_i/\sum (c_i/M_i) \quad (5)$$

where c_i is the protein concentration and M_i is the observed molar mass at the ith slice within an elution profile. It should, however, be noted that R_g could not be determined for any of the protein species because of the lack of angular dependence of scattered light. The time and concentration dependence of dynamic light scattering (DLS) intensity fluctuation of each

dx.doi.org/10.1021/bi3000534 | *Biochemistry* 2012, 51, 2122−2135

protein species resolved in the flow mode was measured by the Wyatt QELS detector positioned at 90° with respect to the incident laser beam. The DLS data were iteratively fit using nonlinear least-squares regression analysis to the following built-in equation in ASTRA:[38−40]

$$G(\tau) = \alpha \exp(-2\Gamma\tau) + \beta \quad (6)$$

where $G(\tau)$ is the autocorrelation function of dynamic light scattering intensity fluctuation I, τ is the delay time of the autocorrelation function, Γ is the decay rate constant of the autocorrelation function, α is the initial amplitude of the autocorrelation function at zero delay time, and β is the baseline offset (the value of the autocorrelation function at an infinite delay time). Thus, fitting eq 6 to a range of $G(\tau)$ versus τ plots as a function of protein concentration along the elution profile of each protein species computes the weight-average value of Γ using DLS measurements at a scattering angle of 90°. Accordingly, the translational diffusion coefficient (D_t) of each protein species was calculated from the following relationship:

$$D_t = (\Gamma\lambda^2)/[16\pi^2 n^2 \sin^2(\theta/2)] \quad (7)$$

where λ is the wavelength of laser light in solution (658 nm), n is the refractive index of the solvent, and θ is the scattering angle (90°). Additionally, the hydrodynamic radius (R_h) of each protein construct was determined from the Stokes−Einstein relationship:

$$R_h = (k_B T)/(6\pi\eta D_t) \quad (8)$$

where k_B is Boltzman's constant (1.38×10^{-23} J K^{-1}), T is the absolute temperature, and η is the solvent viscosity. We note that the R_h reported here represents the weight-average value as defined by the following expression:

$$R_h = \sum (c_i R_{h,i}) / \sum c_i \quad (9)$$

where c_i is the protein concentration and $R_{h,i}$ is the observed hydrodynamic radius at the ith slice within an elution profile. It should also be noted that, in both the SLS and DLS measurements, the protein concentration (c) along the elution profile of each protein species was automatically quantified in ASTRA from the change in the refractive index (Δn) with respect to the solvent as measured by the Wyatt Optilab rEX detector using the following relationship:

$$c = (\Delta n)/(dn/dc) \quad (10)$$

where dn/dc is the refractive index increment of the protein in solution.

Isothermal Titration Calorimetry. Isothermal titration calorimetry (ITC) measurements were performed on a Microcal VP-ITC instrument, and data were acquired and processed using the integrated Microcal ORIGIN software. Briefly, protein samples were prepared in 50 mM Tris, 200 mM NaCl, 1 mM EDTA, and 5 mM β-mercaptoethanol (pH 8.0). The experiments were initiated by injecting 25 × 10 μL aliquots of each construct of the PR domain of Sos1 (0.5−1 mM) from the syringe into the calorimetric cell containing 1.8 mL of a 50−100 μM full-length Grb2 solution at 25 °C. The change in thermal power as a function of each injection was automatically recorded using the ORIGIN software, and the raw data were further processed to yield binding isotherms of heat released per injection as a function of the molar ratio of each PR construct to full-length Grb2. The heats of mixing and dilution were subtracted from the heat of binding per injection by conducting a control experiment in which the same buffer in the calorimetric cell was titrated against each PR construct in an identical manner. To extract the binding affinity (K_d) and binding enthalpy (ΔH), the ITC isotherms were iteratively fit using nonlinear least-squares regression analysis to the following built-in equation in the ORIGIN software:

$$q(i) = [(\Delta HVP)/(2n)](1 + (nL)/P + (nK_d)/P - \{[1 + (nL)/P + (nK_d)/P]^2 - (4nL)/P\}^{1/2}) \quad (11)$$

where $q(i)$ is the heat released (kilocalories per mole) for the ith injection, V is the effective volume of the Grb2 solution in the calorimetric cell (1.46 mL), P is the total concentration of Grb2 in the calorimetric cell, L is the total concentration of each PR construct added from the syringe for the ith injection, and n is the stoichiometry of full-length Grb2 bound to each PR construct at equilibrium. Equation 11 is derived from the binding of a ligand to a macromolecule using the law of mass action assuming a one-site model.[41] The free energy change (ΔG) upon the binding of Grb2 to each PR construct was calculated from the relationship

$$\Delta G = nRT \ln K_d \quad (12)$$

where n is the integral number of binding sites within the PR domain or the observed stoichiometry of binding of Grb2 to the PR domain, R is the universal molar gas constant (1.99 cal K^{-1} mol^{-1}), and T is the absolute temperature. The entropic contribution ($T\Delta S$) to the free energy of binding was calculated from the relationship

$$T\Delta S = \Delta H - \Delta G \quad (13)$$

where ΔH and ΔG are as defined above. Thermodynamic parameters associated with cooperative binding of Grb2 to the observed pairwise combinations of sites S1−S4 within the PR domain of Sos1 with a 2:1 stoichiometry were calculated from the following relationships:

$$\Delta\Delta G_c = \Delta G_{ij} - (\Delta G_i + \Delta G_j) \quad (14)$$

$$\Delta\Delta H_c = \Delta H_{ij} - (\Delta H_i + \Delta H_j) \quad (15)$$

$$T\Delta\Delta S_c = T\Delta S_{ij} - (T\Delta S_i + T\Delta S_j) \quad (16)$$

where $\Delta\Delta H_c$ and $T\Delta\Delta S_c$ are the underlying enthalpic and entropic components to the free energy of cooperativity ($\Delta\Delta G_c$), respectively, the subscript i denotes the corresponding thermodynamic parameters (ΔG_i, ΔH_i, and $T\Delta S_i$) associated with the binding of Grb2 to site i (first site), the subscript j denotes the corresponding thermodynamic parameters (ΔG_j, ΔH_j, and $T\Delta S_j$) associated with the binding of Grb2 to site j (second site), and the subscript ij denotes the corresponding thermodynamic parameters (ΔG_{ij}, ΔH_{ij}, and $T\Delta S_{ij}$) associated with the binding of Grb2 to both sites i and j. ΔG_i, ΔH_i, and $T\Delta S_i$ and ΔG_j, ΔH_j, and $T\Delta S_j$ for each of the four sites (S1−S4) were calculated from the binding of Grb2 to the triple-mutant PR constructs (PR_mS123, PR_mS124, PR_mS134, and PR_mS234). ΔG_{ij}, ΔH_{ij}, and $T\Delta S_{ij}$ for any observed pairwise combination of sites S1−S4 (S1 and S4, S1 and S3, S2 and S4, and S3 and S4) were calculated from the binding of Grb2 to the PR constructs with a 2:1 stoichiometry, namely, the wild-type PR construct (PR_WT), the single-mutant PR constructs (PR_mS1, PR_mS2, PR_mS3, and PR_mS4),

dx.doi.org/10.1021/bi3000534 | Biochemistry 2012, 51, 2122−2135

and the double-mutant PR constructs (PR_mS12, PR_mS13, PR_mS23, and PR_mS24).

Circular Dichroism. Far-UV circular dichroism (CD) measurements were conducted on a Jasco J-815 spectrometer thermostatically controlled at 25 °C. Experiments were conducted with 5 μM wild-type PR domain of Sos1 in 10 mM sodium phosphate (pH 8.0). Data were collected using a quartz cuvette with a 2 mm path length in the 190−250 nm wavelength range. Data were normalized against reference spectra to remove the contribution of buffer. Data were recorded with a slit bandwidth of 2 nm at a scan rate of 10 nm/min. Each data set represents an average of four scans acquired at 0.1 nm intervals. Data were converted to molar ellipticity, $[\theta]$, as a function of wavelength (λ) of electromagnetic radiation using the equation

$$[\theta] = (10^5 \Delta\varepsilon)/(cl) \text{ deg cm}^2 \text{ dmol}^{-1} \quad (17)$$

where $\Delta\varepsilon$ is the observed ellipticity in millidegress, c is the protein concentration in micromolar, and l is the cuvette path length in centimeters.

Molecular Modeling. Molecular modeling (MM) was employed to construct structural models of Grb2 bivalently bound to S1−S4 sites within the PR domain of Sos1 either as two independent monomers (Grb2−PR−Grb2) or in the context of a homodimer ($[Grb2]_2$−PR), using MODELER based on homology modeling.[42] Briefly, the atomic models were built in various stages. First, the intervening polypeptide chain spanning sites S1−S4 within the PR domain of Sos1 was folded into a compact globular-like topology using the QUARK server based on ab initio modeling. The QUARK server can be accessed online at http://zhanglab.ccmb.med.umich.edu/quark. Notably, ab initio modeling was motivated by the fact that the PR domain of Sos1 appears to be structurally compact on the basis of our hydrodynamic data presented here. Next, the $[Grb2]_2$−PR structural model was built using the ab initio structural model of the PR domain in combination with the crystal structure of the Grb2 homodimer alone [Protein Data Bank (PDB) entry 1GRI] and the solution structure of the isolated nSH3 domain of Grb2 bound to a PXψPXR motif homologous to sites S1 and S4 (PDB entry 4GBQ) using the multiple-template alignment strategy in MODELER.[42] Additionally, hydrogen bonding restraints between the consensus arginine (R1156) within site S1 and D15 within the nSH3 domain of one monomer of Grb2 as well as between the consensus arginine (R1295) within site S4 and D15 within the nSH3 domain of the second monomer of Grb2 were introduced as described previously.[43] The Grb2−PR−Grb2 structural model was derived from the prebuilt $[Grb2]_2$−PR structural model. Here, the intervening polypeptide chain spanning sites S1 and S4 within the PR domain of Sos1 was excised, and the two monomers within the Grb2 homodimer bound to isolated S1 and S4 sites were spatially displaced and moved apart laterally in a rigid-body fashion to make them devoid of any intermonomer contacts in MOLMOL.[44] The resulting conformation of two noninteracting Grb2 monomers in complex with isolated S1 and S4 sites in combination with the ab initio structural model of the PR domain was subsequently used as a template to construct the Grb2−PR−Grb2 structural model in MODELER.[42] In each case, a total of 100 structural models were calculated and the structure with the lowest energy, as judged by the MODELER Objective Function, was selected for further analysis. The modeled structures were rendered using RIBBONS.[45] All calculations and data processing were performed on a Linux workstation equipped with a dual-core processor.

Molecular Dynamics. Molecular dynamics (MD) simulations were performed with GROMACS[46,47] using the integrated OPLS-AA force field.[48,49] Briefly, the modeled structures of Grb2 in complex with the PR domain of Sos1 through bivalent binding at sites S1 and S4 as two independent monomers (Grb2−PR−Grb2) or in the context of a homodimer ($[Grb2]_2$−PR) were centered within a cubic box and hydrated using the extended simple point charge (SPC/E) water model.[50,51] The hydrated structures were energy-minimized with the steepest descent algorithm prior to equilibration under the *NPT* ensemble conditions, wherein the number of atoms (N), the pressure (P), and the temperature (T) within the system were kept constant at ~10^5, 1 bar, and 300 K, respectively. The particle mesh Ewald (PME) method was employed to compute long-range electrostatic interactions with a 10 Å cutoff[52] and the Linear Constraint Solver (LINCS) algorithm to restrain bond lengths.[53] All MD simulations were performed under periodic boundary conditions (PBC) using the leapfrog integrator with a time step of 2 fs. For the final MD production runs, data were collected every 10 ps over a time scale of 50 ns. All simulations were run on a Linux workstation using parallel processors at the High Performance Computing facility within the Center for Computational Science of the University of Miami.

RESULTS AND DISCUSSION

The PR Domain of Sos1 Adopts a Monomeric Conformation in Solution. To understand the assembly of the Grb2−Sos1 complex, we first conducted ALS analysis on full-length Grb2 and the PR domain of Sos1 to assess their propensities to associate into higher-order oligomers in solution (Figure 2 and Table 1). Importantly, in addition to the wild-type construct of the PR domain (PR_WT), ALS analysis was also conducted on various single-, double-, and triple-mutant constructs, mutated with respect to one or more of the S1−S4 sites, to determine their effect on the hydrodynamic properties of the PR domain (Figure 1b). Our data suggest that while Grb2 exists in a monomer−dimer equilibrium in agreement with our previous study,[34] the wild-type and various mutant constructs of the PR domain are all monomers in solution. In an attempt to gain insight into the macromolecular polydispersity and shape of the various species, we also determined the corresponding M_w/M_n ratio and hydrodynamic radius (R_h) from our data. Our analysis reveals that both the monomeric and dimeric forms of Grb2 as well as the PR monomers display an M_w/M_n ratio close to unity, implying that they are all highly monodisperse in solution. Furthermore, the hydrodynamic radii observed for the Grb2 monomer and dimer are consistent with their tightly packed $\alpha\beta$ folds.[54]

Remarkably, the hydrodynamic radii observed for the various PR constructs of Sos1 lie somewhere between those of monomeric and dimeric Grb2, implying that the PR domain of Sos1 adopts a compact shape in a manner akin to that adopted by globular proteins rather than an extended random coil-like conformation devoid of any structural features. This observation is particularly surprising in that the proline-rich proteins such as the PR domain of Sos1 are believed to be devoid of any intrinsic structure in solution. This is due to the rigidity of the proline side chain that is structurally destabilizing but nevertheless allows proline-rich proteins to adopt a rigid conformation ideally suited for binding to cognate ligands at

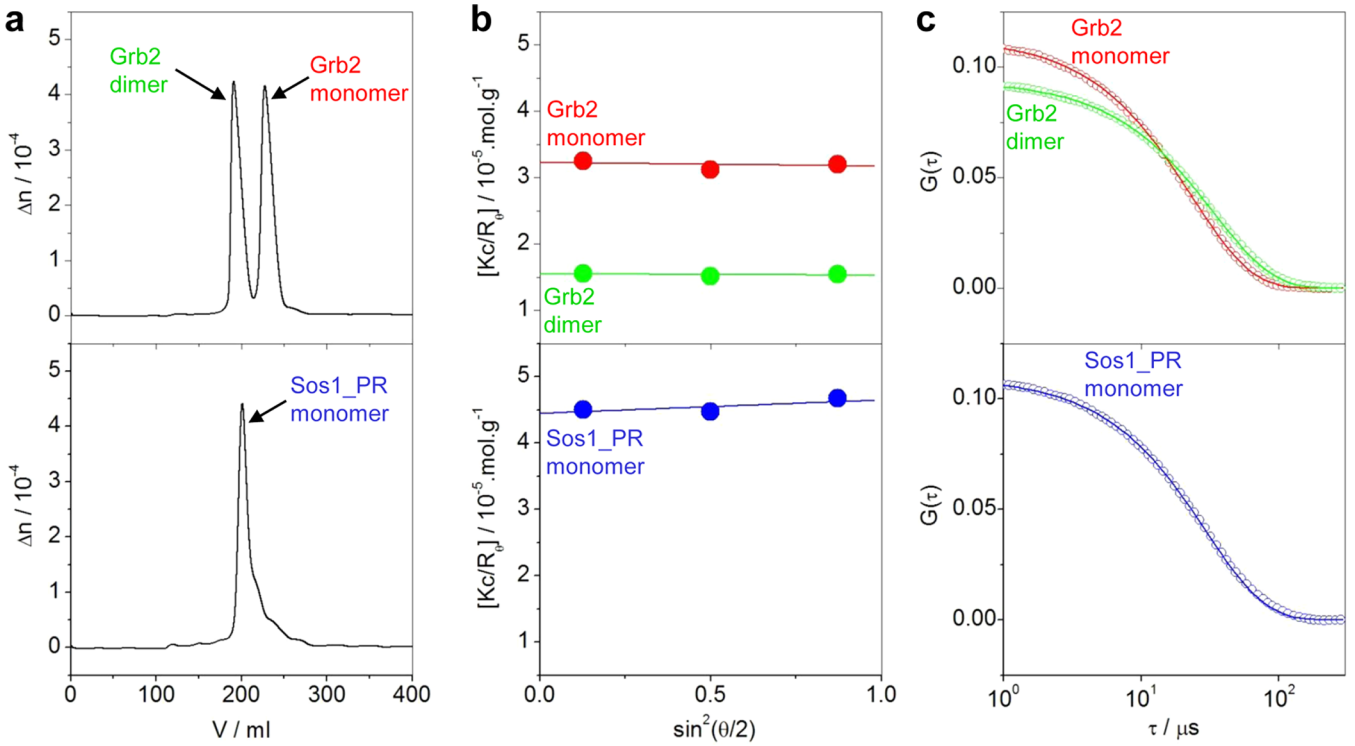

Figure 2. ALS analysis of full-length Grb2 and the PR domain of Sos1 (Sos1_PR). (a) Elution profiles as monitored by the differential refractive index (Δn) plotted as a function of elution volume (V) for Grb2 (top) and Sos1_PR (bottom). Note that Grb2 elutes as two distinct species corresponding to a dimer and a monomer, while the Sos1_PR domain elutes as a single monomeric species. (b) Partial Zimm plots obtained from analytical SLS measurements at a specific protein concentration for the Grb2 dimer and monomer (top) and Sos1_PR monomer (bottom). The solid lines through the data points represent linear fits. (c) Autocorrelation function plots obtained from analytical DLS measurements at a specific protein concentration for the Grb2 dimer and monomer (top) and Sos1_PR monomer (bottom). The solid lines through the data points represent nonlinear least-squares fits to eq 6.

Table 1. Hydrodynamic Parameters Obtained from ALS Measurements for Full-Length Grb2 and Various Constructs of the PR Domain of Sos1[a]

	associativity	M_{cal} (kDa)	M_w (kDa)	M_n (kDa)	M_w/M_n	D_t (μm^2 s^{-1})	R_h (Å)
Grb2	monomer	30	31 ± 1	30 ± 2	1.02 ± 0.03	63 ± 1	39 ± 1
	dimer	60	64 ± 3	63 ± 4	1.01 ± 0.01	45 ± 1	55 ± 2
PR_WT	monomer	22	22 ± 1	22 ± 1	1.00 ± 0.01	53 ± 1	46 ± 1
PR_mS1	monomer	22	21 ± 1	21 ± 1	1.00 ± 0.01	54 ± 1	45 ± 1
PR_mS2	monomer	22	25 ± 1	25 ± 2	1.01 ± 0.01	54 ± 2	45 ± 1
PR_mS3	monomer	22	26 ± 1	25 ± 2	1.03 ± 0.04	50 ± 4	48 ± 3
PR_mS4	monomer	22	22 ± 1	22 ± 2	1.03 ± 0.04	57 ± 4	44 ± 2
PR_mS12	monomer	22	27 ± 1	26 ± 2	1.01 ± 0.01	59 ± 1	42 ± 1
PR_mS13	monomer	22	24 ± 1	23 ± 1	1.05 ± 0.01	58 ± 1	43 ± 1
PR_mS14	monomer	22	24 ± 1	23 ± 2	1.03 ± 0.03	58 ± 3	42 ± 1
PR_mS23	monomer	22	26 ± 1	26 ± 1	1.01 ± 0.01	56 ± 1	44 ± 1
PR_mS24	monomer	22	24 ± 1	24 ± 1	1.01 ± 0.02	57 ± 2	43 ± 1
PR_mS34	monomer	22	25 ± 1	24 ± 1	1.01 ± 0.01	54 ± 1	45 ± 1
PR_mS123	monomer	22	26 ± 1	25 ± 1	1.03 ± 0.03	49 ± 2	50 ± 2
PR_mS124	monomer	22	22 ± 1	22 ± 2	1.01 ± 0.01	55 ± 4	44 ± 3
PR_mS134	monomer	22	23 ± 2	22 ± 3	1.04 ± 0.05	53 ± 3	46 ± 2
PR_mS234	monomer	22	22 ± 1	22 ± 1	1.02 ± 0.02	51 ± 2	47 ± 1

[a]Note that M_{cal} is the molar mass of each recombinant construct calculated from the corresponding amino acid sequence alone. Errors were calculated from at least three independent measurements. All errors are given to one standard deviation.

the expense of little entropic penalty, which is often the bottleneck in protein−protein interactions pertinent to cellular signaling cascades. The fact that the PR domain of Sos1 appears to be compact and globular in solution suggests strongly that the lack of secondary structural elements such as α-helices and β-strands alone may not necessarily equate to a lack of intrinsic structure. On the contrary, our data support the notion that proline-rich proteins may be able to adopt a compact shape and that such adoption may be a necessity to avoid chaos within the cellular environment, where the high concentration of proline-rich sequences and proteins in general may otherwise increase cellular entropy through intrinsic disorder and formation of structural knots.

dx.doi.org/10.1021/bi3000534 | *Biochemistry* 2012, 51, 2122−2135

The PR Domain of Sos1 Is Intrinsically Disordered. The PR domain of Sos1 is abundant in residues such as proline as well as polar and charged residues that are usually found in structurally disordered proteins. Given its key role in the Ras/MAPK pathway, it is fitting that the PR domain of Sos1 shares such a virtue with other structurally disordered proteins believed to play a central role in mediating cellular signaling cascades.[55−59] In an attempt to further analyze the extent of structural disorder within the PR domain of Sos1, we performed secondary structure prediction analysis using POODLE.[60] As shown in Figure 3a, our analysis reveals that

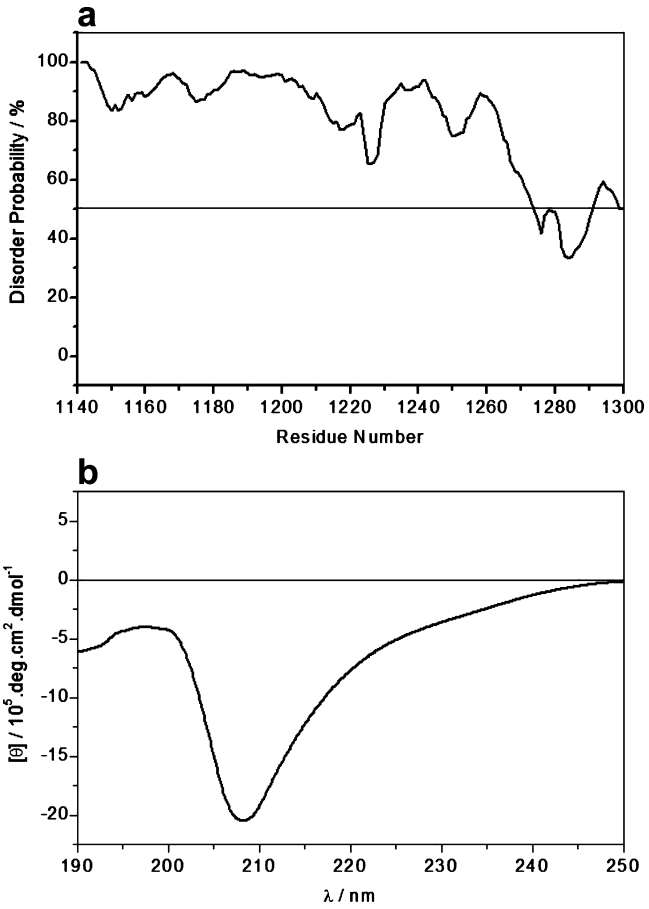

Figure 3. Secondary structure analysis of the PR domain of Sos1. (a) In silico prediction of intrinsic disorder within the PR domain. (b) Experimentally determined far-UV CD spectrum of the PR domain.

the PR domain is indeed predominantly disordered and lacks any identifiable α-helical and/or β-strand features characteristic of well-folded $\alpha\beta$ proteins. This salient observation is further corroborated by our far-UV CD analysis (Figure 3b), wherein the spectrum of the PR domain shows a minimum centered around 208 nm, a signature usually characteristic of proteins containing random coil and polyproline type II (PPII) helical conformations.[61,62] Additionally, the rather broad far-UV CD spectrum of the PR domain suggests that it is conformationally heterogeneous as would be expected for structurally disorderd proteins devoid of a well-defined compact fold.

Grb2 Binds to the PR Domain of Sos1 with a 2:1 Stoichiometry. Although seminal work implicated the role of both SH3 domains of Grb2 in the recruitment of Sos1 to the inner membrane surface,[3,8,17] recent studies have shown that only the nSH3 domain binds to Sos1 in an allosteric manner such that the cSH3 domain is freed up for binding to Gab1 to generate the Sos1−Grb2−Gab1 ternary signaling complex in a noncompetitive fashion.[25,26] Importantly, our previous studies have shown that the isolated nSH3 domain of Grb2 can potentially bind to peptides derived from all four S1−S4 motifs within Sos1 in a physiologically relevant manner.[26,32,33] To understand the stoichiometry and the underlying thermodynamic forces driving the formation of the Grb2−Sos1 signaling complex, we next measured the binding of full-length Grb2 to the PR domain of Sos1 using ITC (representative data are shown in Figure 4 and all data summarized in Table 2). Our analysis reveals that the formation of the Grb2−Sos1 complex is driven by favorable enthalpic changes accompanied by an entropic penalty. This implies that specific intermolecular hydrogen bonding and ion pairing interactions predominate over hydrophobic forces in mediating the association of Grb2 with Sos1 in agreement with our previous reports.[26,32,33]

Of particular note is the observation that Grb2 binds to the wild-type PR domain (PR_WT), containing sites S1−S4, with a 2:1 stoichiometry. In light of previous studies,[25,26] the most straightforward interpretation of this finding is that Grb2 binds in a bivalent manner to Sos1 to form the Grb2−Sos1 complex with a 2:1 stoichiometry and that this interaction is mediated through the binding of the nSH3 domain within each Grb2 molecule to only two of a possible four available S1−S4 sites within Sos1. Given that the PR domain of Sos1 adopts a compact shape and that Grb2 displays the propensity to homodimerize in solution (Figure 2), the 2:1 stoichiometry observed here may not necessarily be due to the binding of the nSH3 domain within each molecule of Grb2 to the PR domain of Sos1. On the contrary, it is highly plausible that the binding of the PR domain through one of its four S1−S4 sites to the nSH3 domain of one monomer within the Grb2 homodimer sterically blocks the binding of the second Grb2 monomer to another PR domain to prevent the formation of the Grb2−Sos1 complex with a 2:2 stoichiometry. To test the extent to which the formation of the Grb2−Sos1 complex with a 2:1 stoichiometry may be influenced by steric hindrance, we next measured the binding of full-length Grb2 to various single-, double-, and triple-mutant constructs of the PR domain, mutated with respect to one or more of the S1−S4 sites (Figure 1 and Table 2). Our data show that Grb2 binds to all single-mutant PR constructs (PR_mS1, PR_mS2, PR_mS3, and PR_mS4) with a 2:1 stoichiometry, implying that none of the four S1−S4 sites is critical for the bivalent binding of Grb2 to Sos1. Remarkably, Grb2 binds in a bivalent manner to only four (PR_mS12, PR_mS13, PR_mS23, and PR_mS24) of the six (PR_mS12, PR_mS13, PR_mS14, PR_mS23, PR_mS24, and PR_mS34) double-mutant PR constructs. This salient observation suggests that bivalent binding of Grb2 to Sos1 can be afforded only by specific pairwise combinations of S1−S4 sites (S1 and S4, S1 and S3, S2 and S4, and S3 and S4) but not others (S1 and S2, and S2 and S3). Close examination of the relative physical location of sites S1−S4 within the PR domain suggests that the length of the intervening linker spanning various pairwise combinations of these sites is likely to play a key role in determining the stoichiometry of the Grb2−Sos1 complex (Figure 1a). Thus, while this intervening linker is comprised of 55−133 residues for the pairwise combinations of sites S1−S4 that favor bivalent binding of Grb2 to Sos1 (S1 and S4, S1 and S3, S2 and S4, and S3 and S4), it merely spans 23−26 residues for the pairwise combinations that result in the formation of the Grb2−Sos1 complex with a 1:1 stoichiometry (S1 and S2, and S2 and S3). The failure of pairwise combinations of sites S1

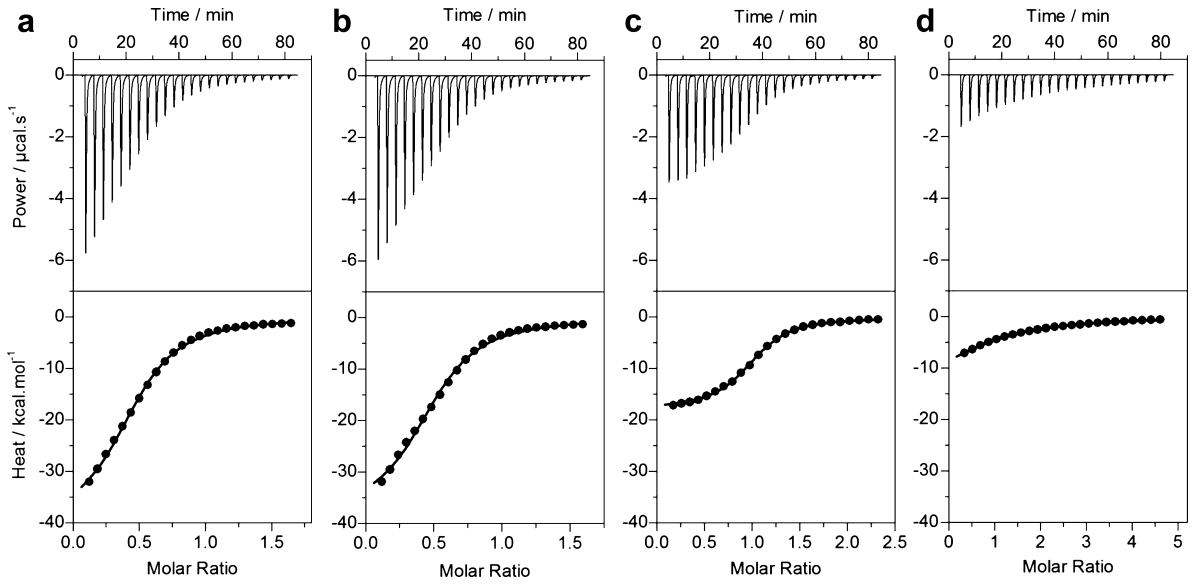

Figure 4. ITC analysis of the binding of full-length Grb2 to the wild-type PR_WT construct (a), the single-mutant PR_mS4 construct (b), the double-mutant PR_mS34 construct (c), and the triple-mutant PR_mS234 construct (d) of Sos1. The top panels show raw ITC data expressed as the change in thermal power with respect to time over the period of titration. In the bottom panels, the change in molar heat is expressed as a function of the molar ratio of the corresponding PR construct to Grb2. The solid lines in the bottom panels show the fit of data to a one-site model, as embodied in eq 11, using the ORIGIN software.

Table 2. Thermodynamic Parameters Obtained from ITC Measurements for the Binding of Wild-Type (WT) and Mutant Constructs of the PR Domain of Sos1 to Full-Length Grb2[a]

	n	K_d (μM)	ΔH (kcal mol^{-1})	$T\Delta S$ (kcal mol^{-1})	ΔG (kcal mol^{-1})
PR_WT	2.12 ± 0.03	7.02 ± 0.04	−39.85 ± 0.28	−25.77 ± 0.29	−14.08 ± 0.01
PR_mS1	1.94 ± 0.01	8.99 ± 0.51	−39.81 ± 0.59	−26.03 ± 0.66	−13.78 ± 0.07
PR_mS2	2.02 ± 0.05	6.98 ± 0.30	−34.11 ± 0.25	−20.03 ± 0.20	−14.08 ± 0.05
PR_mS3	2.04 ± 0.02	2.40 ± 0.03	−38.39 ± 0.33	−23.04 ± 0.32	−15.35 ± 0.01
PR_mS4	2.01 ± 0.02	6.18 ± 0.27	−38.17 ± 0.10	−23.94 ± 0.05	−14.23 ± 0.05
PR_mS12	2.05 ± 0.04	19.57 ± 0.27	−37.06 ± 0.11	−24.20 ± 0.09	−12.86 ± 0.02
PR_mS13	2.14 ± 0.02	10.14 ± 0.05	−36.55 ± 0.08	−22.91 ± 0.08	−13.64 ± 0.01
PR_mS14	1.14 ± 0.01	15.48 ± 0.10	−17.55 ± 0.22	−11.06 ± 0.21	−6.57 ± 0.01
PR_mS23	2.00 ± 0.01	12.67 ± 0.15	−34.56 ± 0.04	−21.18 ± 0.05	−13.37 ± 0.01
PR_mS24	1.89 ± 0.02	11.76 ± 0.70	−32.52 ± 0.64	−19.05 ± 0.71	−13.46 ± 0.07
PR_mS34	1.00 ± 0.01	2.29 ± 0.12	−17.53 ± 0.42	−9.82 ± 0.44	−7.70 ± 0.03
PR_mS123	1.07 ± 0.05	37.28 ± 3.62	−20.09 ± 0.03	−14.04 ± 0.03	−6.05 ± 0.06
PR_mS124	1.03 ± 0.04	101.44 ± 2.04	−14.61 ± 0.13	−9.15 ± 0.12	−5.45 ± 0.01
PR_mS134	1.05 ± 0.01	29.98 ± 1.65	−18.14 ± 0.25	−11.96 ± 0.28	−6.18 ± 0.03
PR_mS234	1.03 ± 0.02	44.96 ± 1.29	−16.88 ± 0.12	−10.94 ± 0.10	−5.94 ± 0.02

[a]Note that n is the stoichiometry of full-length Grb2 bound to each PR construct. Errors were calculated from at least three independent measurements. All errors are given to one standard deviation.

and S2 and sites S2 and S3, to afford bivalent binding of Grb2 to Sos1 thus most likely results from steric hindrance in that binding of one molecule of Grb2 to site S1 physically blocks the binding of a second molecule of Grb2 to site S2 and vice versa. In a similar manner, binding of one molecule of Grb2 to site S2 would be expected to physically block the binding of a second molecule of Grb2 to site S3 and vice versa. Finally, Grb2 binds to all four triple-mutant PR constructs with a 1:1 stoichiometry (PR_mS123, PR_mS124, PR_mS134, and PR_mS234). This finding strongly argues that the formation of the Grb2−Sos1 complex with a 2:1 stoichiometry is not due to steric hindrance and that it strictly requires the integrity of at least two native sites in one of the four pairwise combinations (S1 and S4, S1 and S3, S2 and S4, and S3 and S4).

Role of Facilitated Diffusion in the Formation of the Grb2−Sos1 Complex. Within the living cell, multivalent binding has evolved as a common mechanism for augmenting the affinity and specificity of macromolecular interactions. Such enhancement is possible not only because intermolecular binding at one site increases the effective local concentration at the second site but also because subsequent intramolecular binding lowers the entropic penalty. Interestingly, our ITC data suggest that binding of Grb2 to two or more sites within the PR domain of Sos1 does not necessarily have to be mutually inclusive to enhance the affinity and specificity of macromolecular interactions (Table 2). Thus, for example, Grb2 binds in a monovalent manner to the double-mutant PR_mS14 construct with an affinity that is comparable to that observed

dx.doi.org/10.1021/bi3000534 | Biochemistry 2012, 51, 2122−2135

for bivalent binding to double-mutant PR_mS12, PR_mS13, PR_mS23, and PR_mS24 constructs and, apparently, only marginally weaker than affinities associated with bivalent binding to the wild-type (PR_WT) and single-mutant constructs (PR_mS1, PR_mS2, PR_mS3, and PR_mS4). In other words, bivalent binding seemingly does not result in any enhancement in binding affinity relative to that of monovalent binding of Grb2 to the PR_mS14 construct containing two native sites. The fact that this is so is further corroborated by the observation that the monovalent binding of Grb2 to the double-mutant PR_mS34 construct is stronger than bivalent binding to any of the PR constructs analyzed here. In a remarkable contrast, our analysis of triple-mutant constructs of the PR domain (PR_mS123, PR_mS124, PR_mS134, and PR_mS234) reveals that monovalent binding of Grb2 is up to an order of magnitude weaker relative than bivalent binding to PR constructs with two or more potential binding sites. The observation that monovalent binding is weaker than bivalent binding when the number of potential sites within the PR constructs is reduced to one but comparable and somewhat stronger than bivalent binding when more than one potential site is available unequivocally implicates the role of facilitated diffusion in mediating Grb2−Sos1 interaction.

In thermodynamic terms, Grb2 appears to be in equilibrium exchange between a bound state in association with the PR domain and a free state in solution. The presence of multiple binding sites within the PR domain likely facilitates hopping of Grb2 between these sites in a flip-flop fashion, and such physically mediated rapid exchange, as opposed to slow random diffusion in solution, accounts for high-affinity binding. In the presence of only one potential site within the PR domain, this equilibrium exchange occurs slowly because as Grb2 dissociates from one molecule of the PR domain, the random search for a second potential site to reassociate will likely be met by a separate molecule of the PR domain, and such a scenario will slow the rate of exchange between the bound state and free state, thereby drastically reducing the affinity of Grb2 for PR constructs that contain only a single potential binding site. In contrast, when more than one potential site within the PR domain is available, dissociation from one site will likely result in rapid reassociation or exchange with a second potential site because of its spatial proximity as well as enhanced collisional probability through facilitated diffusion leading to high-affinity binding. However, if the two potential sites are not in steric hindrance with respect to the spatial accessibility of Grb2, then binding will likely occur in a bivalent manner, wherein the exchange between the bound and free states will also be rapid for the reasons discussed above. Taken collectively, our data suggest that bivalent binding is not a prerequisite for an enhancement in the affinity of binding and that monovalent binding through a flip-flop mechanism can also account for such synergy given the availability of multiple binding sites to increase the exchange rate through facilitated diffusion. Strikingly, our data also suggest that ligand binding to two potential sites through monovalent binding in a flip-flop manner may be accompanied by a higher affinity than bivalent binding. We believe that this scenario can be ascribed to the unfavorable entropic factors associated with bivalent binding but not monovalent binding through a flip-flop mechanism.

Bivalent Binding of Grb2 to Sos1 Is Governed by Positive Cooperativity. Our ITC data suggest that bivalent binding of Grb2 to multiple sites within the PR domain of Sos1 results in enhancement of binding affinity by up to an order of magnitude relative to monovalent binding in the context of the availability of a single site (Table 2). The fact that this is so strongly implicates the role of positive cooperativity in driving the assembly of the Grb2−Sos1 signaling complex. In other words, binding at one site enhances binding at a second site in a synergistic manner such that the overall free energy associated with binding at both sites is greater than the sum of free energies associated with binding at each site individually. To shed further light on the nature of these cooperative interactions, we calculated the free energy of cooperativity ($\Delta\Delta G_c$) associated with bivalent binding at each potential pairwise combination of sites S1−S4 within the PR domain as well as the underlying enthalpic ($\Delta\Delta H_c$) and entropic ($T\Delta\Delta S_c$) components associated with such cooperativity (Table 3). Our analysis reveals that $\Delta\Delta G_c$ associated with bivalent binding of Grb2 to the PR domain ranges from −1.36 to −3.36 kcal/mol. More importantly, the origin of this favorable $\Delta\Delta G_c$ lies in both enthalpic and entropic components. For example, bivalent binding at sites S1 and S4, S1 and S3, and S3 and S4 within the PR_WT construct is driven by a favorable $\Delta\Delta H_c$ accompanied by an unfavorable $T\Delta\Delta S_c$, while bivalent binding at sites S2 and S4 is favored by both $\Delta\Delta H_c$ and $T\Delta\Delta S_c$. On the other hand, bivalent binding at sites S2 and S4 and sites S1 and S4 within the PR_mS13 and PR_mS23 constructs, respectively, is largely governed by a favorable $T\Delta\Delta S_c$ accompanied by an unfavorable $\Delta\Delta H_c$. These salient observations indicate that the positive cooperativity associated with bivalent binding of Grb2 to the PR domain of Sos1 arises through both the formation of additional intermolecular contacts (favorable enthalpy) and the burial of additional hydrophobic surfaces (favorable entropy). We also note that the favorable entropic contributions to the overall free energy of cooperativity are also likely to arise from the rapid exchange of Grb2 between multiple sites within the PR domain through facilitated diffusion. This invokes the

Table 3. Thermodynamic Parameters Associated with Cooperative Binding of Full-Length Grb2 to Wild-Type (WT) and Various Mutant Constructs of the PR Domain of Sos1 with a 2:1 Stoichiometry[a]

	bivalent sites	$\Delta\Delta H_c$ (kcal mol^{-1})	$T\Delta\Delta S_c$ (kcal mol^{-1})	$\Delta\Delta G_c$ (kcal mol^{-1})
PR_WT	S1 and S4	−2.88	−0.79	−2.09
	S1 and S3	−8.36	−5.68	−2.69
	S2 and S4	−1.62	0.23	−1.85
	S3 and S4	−5.15	−2.58	−2.58
PR_mS1	S2 and S4	−1.58	−0.03	−1.55
	S3 and S4	−5.11	−2.84	−2.28
PR_mS2	S1 and S4	2.86	4.95	−2.09
	S1 and S3	−2.62	0.06	−2.69
	S3 and S4	0.59	3.16	−2.58
PR_mS3	S1 and S4	−1.42	1.94	−3.36
	S2 and S4	−0.16	2.96	−3.12
PR_mS4	S1 and S3	−6.68	−3.85	−2.84
PR_mS12	S3 and S4	−2.36	−1.01	−1.36
PR_mS13	S2 and S4	1.68	3.08	−1.41
PR_mS23	S1 and S4	2.41	3.80	−1.38
PR_mS24	S1 and S3	−1.03	1.04	−2.07

[a]Note that thermodynamic parameters associated with cooperativity are provided for all observed pairwise combinations of sites S1−S4 within each PR construct to which Grb2 may bind in a bivalent manner.

possibility that although Grb2 can occupy a maximum of only two sites within the PR domain at any one moment, nonoccupied sites are likely involved in modulating this protein−protein interaction.

Structural Basis of the Binding of Grb2 to the PR Domain of Sos1 as Two Independent Monomers versus a Homodimer. Our thermodynamic data suggest that the bivalent binding of Grb2 to Sos1 with a 2:1 stoichiometry is under cooperative control in that the binding of the nSH3 domain within one Grb2 molecule to one of the S1−S4 sites within Sos1 facilitates the binding of the nSH3 domain within a second Grb2 molecule. On the other hand, our hydrodynamic data indicate that Grb2 exists in a monomer−dimer equilibrium in solution. In light of these observations, it is thus conceivable that Grb2 could bind to the PR domain of Sos1 either as two independent monomers (Grb2−PR−Grb2) or alternatively as a homodimer ($[Grb2]_2$−PR). To gain insight into the structural basis of the binding of Grb2 to Sos1 as two independent monomers and to compare this mode of binding to that of a homodimer, we built appropriate structural models of Grb2 bivalently bound to PXψPXR motifs located within sites S1 and S4 in the PR domain of Sos1 (Figure 5). Our structural models suggest that the canonical hydrophobic grooves within the nSH3 domains of Grb2 that accommodate the PXψPXR motifs are fully exposed to solution in the context of both the monomers (Figure 5a) and the homodimer (Figure 5b), implying that it is indeed physically feasible for Grb2 to bind to the PR domain as two independent monomers or as a homodimer. Importantly, the monomers within the Grb2 homodimer adopt a 2-fold axis of symmetry such that the SH2 domain of one monomer docks against the cSH3 domain of the other and vice versa in a head-to-tail fashion as observed in the crystal structure determined by Ducruix and co-workers.[54]

Our structural modeling also reveals that each PXψPXR motif located within sites S1 and S4 latches onto the hydrophobic groove running parallel to the RT loop within the β-barrel fold of each nSH3 domain and adopts a left-handed PPII helical conformation in a canonical fashion.[27−30] Within each nSH3 hydrophobic groove, the PXψPXR motifs are stabilized by an extensive network of intermolecular contacts as reported previously.[26,32,33] In particular, the aliphatic side chains of the consensus ψ residue within sites S1 (V1153) and S4 (V1292) are sandwiched between benzyl rings of F9 and Y52 located within each nSH3 hydrophobic groove through van der Waals contacts. Additionally, the guanidine moieties of the consensus arginine within sites S1 (R1156) and S4 (R1295) form hydrogen bonds and/or ion pairs with the carboxylic groups of D15 located within each nSH3 hydrophobic groove. Importantly, the aliphatic side chains of R1156 (S1) and R1295 (S4) are further stabilized through van der Waals contacts with the indole moieties of W36 located within each nSH3 hydrophobic groove.

We add that although the spatial orientations of both PXψPXR motifs relative to the nSH3 domains within Grb2 monomers or the homodimer can be relied upon with a high degree of confidence at the atomic level, because they were modeled on the basis of a high level of sequence identity with corresponding templates, there is a high probability of uncertainty in the relative orientation and conformation of the intervening polypeptide chain spanning sites S1 and S4 within the PR domain of Sos1. Notably, this intervening polypeptide chain was folded into a compact globular-like topology, in agreement with our hydrodynamic data, on the basis of ab initio modeling without any template. Despite such shortcomings, our structural models lend physical insight into the bivalent binding of the Grb2 adaptor to the Sos1 guanine nucleotide exchange factor and provide a much anticipated structural framework for further understanding the assembly of this key signaling complex.

MD Simulations Support the Binding of Grb2 to the PR Domain of Sos1 as a Homodimer in Lieu of Two Independent Monomers. In an attempt to test the validity of our structural models and to shed light on macromolecular dynamics underlying the assembly of the Grb2−Sos1 signaling complex, we performed MD simulations on structural models of Grb2 bivalently bound to PXψPXR motifs located within sites S1 and S4 in the PR domain of Sos1 either as two independent monomers (Grb2−PR−Grb2) or alternatively as a homodimer ($[Grb2]_2$−PR) (Figure 6). Importantly, we assessed the stability and dynamics of various complexes and their constituent components in terms of both the root-mean-square deviation (rmsd) of backbone atoms as a function of simulation time and root-mean-square fluctuation (rmsf) of backbone atoms as a function of residue number along each protein chain. As shown in Figure 6a, the MD trajectories reveal that while the $[Grb2]_2$−PR complex reaches structural equilibrium with an rmsd of ∼7 Å after ∼30 ns, the Grb2−PR−Grb2 complex displays structural instability with a continually increasing rmsd of >15 Å even after 50 ns of simulation time. Simply put, these observations strongly argue that the Grb2 homodimer bound to the PR domain of Sos1 is structurally more stable than Grb2 monomers.

To understand the origin of such differential structural stabilities, we next deconvoluted the overall rmsd of each complex into its three constituent components: the PR domain of Sos1 and Grb2 monomers, designated MonA and MonB. Remarkably, our analysis reveals that the PR domain and Grb2 monomers individually are also much more structurally stable in the context of the $[Grb2]_2$−PR complex than in the Grb2−PR−Grb2 complex. Thus, while Grb2 monomers in the context of a Grb2 homodimer bound to the PR domain display relatively high stability with an rmsd of ∼1.5 Å over the entire course of the MD simulation, they appear to be unstable with an rmsd of ∼3 Å when bound to the PR domain as two independent monomers. Additionally, while the PR domain in the context of the $[Grb2]_2$−PR complex reaches structural equilibrium with an rmsd of ∼10 Å after ∼30 ns, the PR domain in the context of the Grb2−PR−Grb2 complex remains structurally unstable with an rmsd of >15 Å. The distinctly higher structural stabilities of the PR domain of Sos1 and Grb2 monomers in the context of the $[Grb2]_2$−PR complex are further demonstrated through our rmsf analysis (Figure 6b), wherein the distribution of atomic fluctuations within each residue of the corresponding protein chain is monitored over the entire course of the MD simulation. Thus, while a majority of residues within Grb2 monomers in the context of the $[Grb2]_2$−PR complex fluctuate with an rmsf of <2 Å, this value increases to >5 Å in the context of the Grb2−PR−Grb2 complex. Strikingly, our rmsf analysis also reveals that the residues within the PR domain of Sos1 in the context of the $[Grb2]_2$−PR complex display smaller fluctuations than those in the context of the Grb2−PR−Grb2 complex (Figure 6c).

We note that one possibility for the rather large distance deviations and fluctuations observed for the Grb2−PR−Grb2 complex may be due to the highly flexible nature of the PR domain tethering the Grb2 monomers. Additionally, Grb2 monomers

dx.doi.org/10.1021/bi3000534 | Biochemistry 2012, 51, 2122−2135

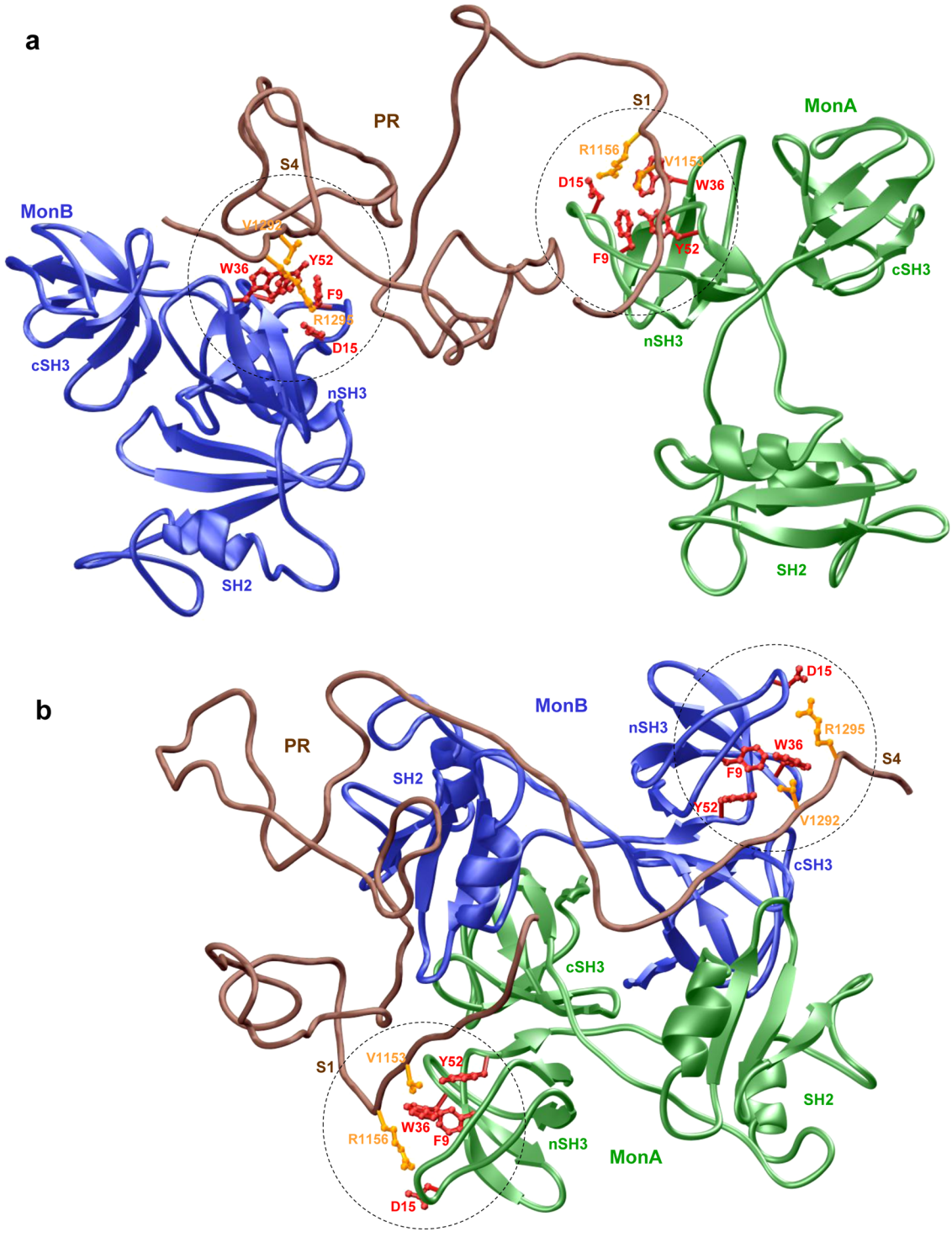

Figure 5. Structural models of Grb2 bound to sites S1 and S4 within the PR domain of Sos1 either as two isolated monomers, Grb2−PR−Grb2 (a), or in the context of a homodimer, $[Grb2]_2$−PR (b). One monomer of Grb2 is colored green (MonA) and the other blue (MonB). The PR domain of Sos1 is colored brown. The Grb2−Sos1 interfaces between the hydrophobic grooves within the nSH3 domains of Grb2 monomers accommodating the PXψPXR motifs within sites S1 and S4 are marked by dashed circles. The side chain moieties of ψ and arginine residues within the PXψPXR motifs at sites S1 and S4 are colored yellow. The side chian moieties of residues within the nSH3 domains of Grb2 that interact with ψ and arginine residues within the PXψPXR motifs are colored red.

in isolation are also likely to be more dynamic than in the context of the Grb2 dimer alone or when bound to the PR domain. Our previous studies have indeed shown that Grb2 monomers most likely undergo structural rearrangement, with respect to the spatial orientation of various domains within the nSH3-SH2-cSH3 modular cassette, to adopt a conformation that is somewhat topologically distinct from and thermodynamically more stable than that observed in the context of the Grb2 homodimer.[34] In an attempt to overcome the additional instability introduced by the rather large intervening linker (~130 residues) spanning sites S1 and S4 within the PR domain, we also performed MD simulations on Grb2 monomers

dx.doi.org/10.1021/bi3000534 | *Biochemistry* 2012, 51, 2122−2135

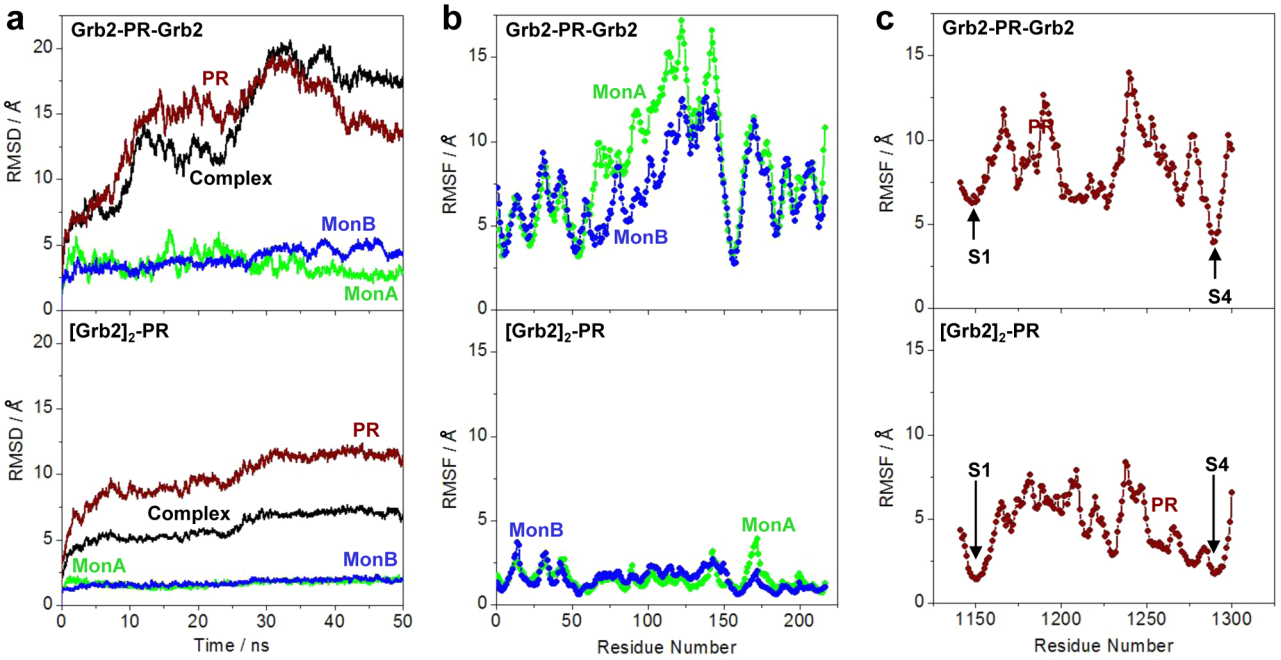

Figure 6. MD analysis of Grb2 bound to sites S1 and S4 within the PR domain of Sos1 either as two independent monomers (Grb2−PR−Grb2) or in the context of a homodimer ($[Grb2]_2$−PR). (a) Root-mean-square deviations (rmsds) of backbone atoms (N, Cα, and C) within each simulated structure relative to the initial modeled structures of Grb2−PR−Grb2 (top) and $[Grb2]_2$−PR (bottom) complexes as a function of simulation time. Note that the overall rmsd for each complex (black) is deconvoluted into the PR domain (brown) and each of the two Grb2 monomers, designated MonA (green) and MonB (blue). (b) Root-mean-square fluctuations (rmsfs) of backbone atoms (N, Cα, and C) averaged over the entire course of corresponding MD trajectories of Grb2−PR−Grb2 (top) and $[Grb2]_2$−PR (bottom) complexes as a function of residue number within each of the two Grb2 monomers, designated MonA (green) and MonB (blue). (c) Root-mean-square fluctuations (rmsfs) of backbone atoms (N, Cα, and C) averaged over the entire course of corresponding MD trajectories of Grb2−PR−Grb2 (top) and $[Grb2]_2$−PR (bottom) complexes as a function of residue number within the PR domain (brown). Note that the vertical arrows indicate the location of sites S1 and S4 within the PR domain.

in isolation and in the context of the Grb2 dimer in complex with PR polypeptides spanning sites S1 and S2 and sites S2 and S3, which harbor rather shorter intervening linkers (~20 residues). Our results nonetheless reach a similar conclusion: both the PR domain and Grb2 monomers display higher structural stability within the $[Grb2]_2$−PR complex than within the Grb2−PR−Grb2 complex. Taken together, our MD analysis suggests that the $[Grb2]_2$−PR complex is structurally more stable than the Grb2−PR−Grb2 complex, though the possibility that Grb2 may bind to the PR domain as isolated monomers as effectively as a homodimer cannot be excluded.

CONCLUSIONS

In response to mitogenic stimulation of RTKs, the Grb2−Sos1 interaction facilitates the activation of Ras GTPase and Akt kinase that in turn drive a plethora of cellular signaling cascades central to health and disease.[1−4] Despite such urgency, the assembly of the Grb2−Sos1 signaling complex remains poorly understood in mechanistic terms. Although structural studies provided insights into how the nSH3 domain of Grb2 recognizes the PXψPXR motifs within Sos1 more than a decade ago,[27−31] further progress in elucidating how these two proteins come together has been largely hampered by the flexible nature of the PR domain of Sos1. Herein, our biophysical analysis sheds new light on the assembly of the Grb2−Sos1 signaling complex at the macromolecular level.

We have demonstrated here that the formation of the Grb2−Sos1 signaling complex occurs with a 2:1 stoichiometry in agreement with previous studies reported by Samelson and coworkers.[63] Of particular note is the observation that Grb2 binds in a bivalent manner to pairwise combinations of sites S1 and S4, S1 and S3, S2 and S4, and S3 and S4 within the PR domain of Sos1 but not to sites S1 and S2 and sites S2 and S3. We attribute the inability of Grb2 to bind to pairwise combinations of sites S1 and S2 and sites S2 and S3 in a bivalent manner to the physical constraints arising from the rather shorter length of the intervening linker spanning these sites relative to other pairwise combinations. Nonetheless, the demonstration that the bivalent binding of Grb2 to Sos1 through a variety of pairwise combinations of sites S1−S4 is feasible strongly argues that conformational heterogeneity may be a hallmark of the Grb2−Sos1 signaling complex, formation of conformationally distinct complexes through the employment of distinct pairwise combinations of sites S1−S4. We believe that such conformational heterogeneity may be an important regulator of the cellular signaling cascades under the control of the Grb2−Sos1 complex. Thus, for example, binding of Grb2 to one or more of the S1−S4 sites may be blocked through post-translational modification of these sites within certain tissue types, which in turn could provide a mechanism for gauging the conformational heterogeneity of the Grb2−Sos1 complex. Alternatively, binding of other cellular partners within the vicinity of sites S1−S4 may also sterically hinder the extent to which Grb2 can recognize these sites and thereby fine-tune the degree of conformational heterogeneity of the Grb2−Sos1 complex. More importantly, within the living cell, multivalent binding has evolved as a common mechanism for augmenting the affinity and specificity of macromolecular interactions. Remarkably, our data suggest that bivalent binding is not a prerequisite for an enhancement of the affinity of binding and that

dx.doi.org/10.1021/bi3000534 | *Biochemistry* 2012, 51, 2122−2135

monovalent binding in a flip-flop fashion can also lead to such enhancement given the availability of multiple binding sites to increase the exchange rate through facilitated diffusion. Our structural models in combination with MD simulations suggest that although it is physically feasible for Grb2 to bind to Sos1 as two independent monomers, it most likely does so as a homodimer. This scenario is further consistent with our finding that the formation of the Grb2−Sos1 complex is governed by positive cooperativity: binding of the nSH3 domain within one monomer of Grb2 to Sos1 facilitates binding of the nSH3 domain within the second monomer of Grb2.

In short, our study provides new insight into the assembly of a key protein−protein interaction central to cellular machinery and argues for a better understanding of the role of multivalent interactions and flip-flop binding coupled with facilitated diffusion and cooperativity in driving cellular signaling cascades central to health and disease. Importantly, current strategies for the rational development of next-generation therapies are based on tethering two potential inhibitors with the intent of enhancing target specificity. Our findings presented here suggest that the design of drugs that can potentially exploit the flip-flop mechanism may provide an alternative and perhaps even more robust strategy for the treatment of disease with more streamlined efficacy coupled with low toxicity.

AUTHOR INFORMATION

Corresponding Author

*E-mail: amjad@farooqlab.net. Telephone: (305) 243-2429. Fax: (305) 243-3955.

Funding

This work was supported by funds from the National Institutes of Health (Grant R01-GM083897) and the USylvester Braman Family Breast Cancer Institute to A.F. C.B.M. is a recipient of a postdoctoral fellowship from the National Institutes of Health (T32-CA119929).

Notes

The authors declare no competing financial interest.

ABBREVIATIONS

ALS, analytical light scattering; CD, circular dichroism; DLS, dynamic light scattering; EGF, epidermal growth factor; Gab1, Grb2-associated binder 1; Grb2, growth factor receptor binder 2; ITC, isothermal titration calorimetry; LIC, ligation-independent cloning; MAP, mitogen-activated protein; MAPK, mitogen-activated protein kinase; MD, molecular dynamics; MM, molecular modeling; PDGF, platelet-derived growth factor; PPII, polyproline type II; PR, proline-rich; RTK, receptor tyrosine kinase; SEC, size-exclusion chromatography; SH2, Src homology 2; SH3, Src homology 3; SLS, static light scattering; Sos1, son of sevenless 1.

REFERENCES

(1) Chardin, P., Cussac, D., Maignan, S., and Ducruix, A. (1995) The Grb2 adaptor. *FEBS Lett. 369*, 47−51.

(2) Nimnual, A., and Bar-Sagi, D. (2002) The two hats of SOS. *Sci. STKE 2002*, PE36.

(3) Li, N., Batzer, A., Daly, R., Yajnik, V., Skolnik, E., Chardin, P., Bar-Sagi, D., Margolis, B., and Schlessinger, J. (1993) Guanine-nucleotide-releasing factor hSos1 binds to Grb2 and links receptor tyrosine kinases to Ras signalling. *Nature 363*, 85−88.

(4) Gale, N. W., Kaplan, S., Lowenstein, E. J., Schlessinger, J., and Bar-Sagi, D. (1993) Grb2 mediates the EGF-dependent activation of guanine nucleotide exchange on Ras. *Nature 363*, 88−92.

(5) Rozakis-Adcock, M., McGlade, J., Mbamalu, G., Pelicci, G., Daly, R., Li, W., Batzer, A., Thomas, S., Brugge, J., Pelicci, P. G., et al. (1992) Association of the Shc and Grb2/Sem5 SH2-containing proteins is implicated in activation of the Ras pathway by tyrosine kinases. *Nature 360*, 689−692.

(6) Rozakis-Adcock, M., Fernley, R., Wade, J., Pawson, T., and Bowtell, D. (1993) The SH2 and SH3 domains of mammalian Grb2 couple the EGF receptor to the Ras activator mSos1. *Nature 363*, 83−85.

(7) Lowenstein, E. J., Daly, R. J., Batzer, A. G., Li, W., Margolis, B., Lammers, R., Ullrich, A., Skolnik, E. Y., Bar-Sagi, D., and Schlessinger, J. (1992) The SH2 and SH3 domain-containing protein GRB2 links receptor tyrosine kinases to ras signaling. *Cell 70*, 431−442.

(8) Chardin, P., Camonis, J. H., Gale, N. W., van Aelst, L., Schlessinger, J., Wigler, M. H., and Bar-Sagi, D. (1993) Human Sos1: A guanine nucleotide exchange factor for Ras that binds to GRB2. *Science 260*, 1338−1343.

(9) Schaeper, U., Gehring, N. H., Fuchs, K. P., Sachs, M., Kempkes, B., and Birchmeier, W. (2000) Coupling of Gab1 to c-Met, Grb2, and Shp2 mediates biological responses. *J. Cell Biol. 149*, 1419−1432.

(10) Lewitzky, M., Kardinal, C., Gehring, N. H., Schmidt, E. K., Konkol, B., Eulitz, M., Birchmeier, W., Schaeper, U., and Feller, S. M. (2001) The C-terminal SH3 domain of the adapter protein Grb2 binds with high affinity to sequences in Gab1 and SLP-76 which lack the SH3-typical P-x-x-P core motif. *Oncogene 20*, 1052−1062.

(11) Seedorf, K., Kostka, G., Lammers, R., Bashkin, P., Daly, R., Burgess, W. H., van der Bliek, A. M., Schlessinger, J., and Ullrich, A. (1994) Dynamin binds to SH3 domains of phospholipase C γ and GRB-2. *J. Biol. Chem. 269*, 16009−16014.

(12) Vidal, M., Montiel, J. L., Cussac, D., Cornille, F., Duchesne, M., Parker, F., Tocque, B., Roques, B. P., and Garbay, C. (1998) Differential interactions of the growth factor receptor-bound protein 2 N-SH3 domain with son of sevenless and dynamin. Potential role in the Ras-dependent signaling pathway. *J. Biol. Chem. 273*, 5343−5348.

(13) Odai, H., Sasaki, K., Iwamatsu, A., Hanazono, Y., Tanaka, T., Mitani, K., Yazaki, Y., and Hirai, H. (1995) The proto-oncogene product c-Cbl becomes tyrosine phosphorylated by stimulation with GM-CSF or Epo and constitutively binds to the SH3 domain of Grb2/Ash in human hematopoietic cells. *J. Biol. Chem. 270*, 10800−10805.

(14) Park, R. K., Kyono, W. T., Liu, Y., and Durden, D. L. (1998) CBL-GRB2 interaction in myeloid immunoreceptor tyrosine activation motif signaling. *J. Immunol. 160*, 5018−5027.

(15) Moeller, S. J., Head, E. D., and Sheaff, R. J. (2003) p27Kip1 inhibition of GRB2-SOS formation can regulate Ras activation. *Mol. Cell. Biol. 23*, 3735−3752.

(16) Adams, J. A., McGlone, M. L., Gibson, R., and Taylor, S. S. (1995) Phosphorylation modulates catalytic function and regulation in the cAMP-dependent protein kinase. *Biochemistry 34*, 2447−2454.

(17) Egan, S. E., Giddings, B. W., Brooks, M. W., Buday, L., Sizeland, A. M., and Weinberg, R. A. (1993) Association of Sos Ras exchange protein with Grb2 is implicated in tyrosine kinase signal transduction and transformation. *Nature 363*, 45−51.

(18) Reuther, G. W., and Der, C. J. (2000) The Ras branch of small GTPases: Ras family members don't fall far from the tree. *Curr. Opin. Cell Biol. 12*, 157−165.

(19) Robinson, M. J., and Cobb, M. H. (1997) Mitogen-activated protein kinase pathways. *Curr. Opin. Cell Biol. 9*, 180−186.

(20) Cunnick, J. M., Meng, S., Ren, Y., Desponts, C., Wang, H. G., Djeu, J. Y., and Wu, J. (2002) Regulation of the mitogen-activated protein kinase signaling pathway by SHP2. *J. Biol. Chem. 277*, 9498−9504.

(21) Gu, H., and Neel, B. G. (2003) The "Gab" in signal transduction. *Trends Cell Biol. 13*, 122−130.

(22) Araki, T., Nawa, H., and Neel, B. G. (2003) Tyrosyl phosphorylation of Shp2 is required for normal ERK activation in response to some, but not all, growth factors. *J. Biol. Chem. 278*, 41677−41684.

(23) Yart, A., Laffargue, M., Mayeux, P., Chretien, S., Peres, C., Tonks, N., Roche, S., Payrastre, B., Chap, H., and Raynal, P. (2001)

A critical role for phosphoinositide 3-kinase upstream of Gab1 and SHP2 in the activation of ras and mitogen-activated protein kinases by epidermal growth factor. *J. Biol. Chem. 276*, 8856−8864.
(24) Kim, D., and Chung, J. (2002) Akt: Versatile mediator of cell survival and beyond. *J. Biochem. Mol. Biol. 35*, 106−115.
(25) Ong, S. H., Hadari, Y. R., Gotoh, N., Guy, G. R., Schlessinger, J., and Lax, I. (2001) Stimulation of phosphatidylinositol 3-kinase by fibroblast growth factor receptors is mediated by coordinated recruitment of multiple docking proteins. *Proc. Natl. Acad. Sci. U.S.A. 98*, 6074−6079.
(26) McDonald, C. B., Seldeen, K. L., Deegan, B. J., Bhat, V., and Farooq, A. (2010) Assembly of the Sos1-Grb2-Gab1 ternary signaling complex is under allosteric control. *Arch. Biochem. Biophys. 494*, 216−225.
(27) Wittekind, M., Mapelli, C., Farmer, B. T. II, Suen, K. L., Goldfarb, V., Tsao, J., Lavoie, T., Barbacid, M., Meyers, C. A., and Mueller, L. (1994) Orientation of peptide fragments from Sos proteins bound to the N-terminal SH3 domain of Grb2 determined by NMR spectroscopy. *Biochemistry 33*, 13531−13539.
(28) Wittekind, M., Mapelli, C., Lee, V., Goldfarb, V., Friedrichs, M. S., Meyers, C. A., and Mueller, L. (1997) Solution structure of the Grb2 N-terminal SH3 domain complexed with a ten-residue peptide derived from SOS: Direct refinement against NOEs, J-couplings and ^{1}H and ^{13}C chemical shifts. *J. Mol. Biol. 267*, 933−952.
(29) Goudreau, N., Cornille, F., Duchesne, M., Parker, F., Tocque, B., Garbay, C., and Roques, B. P. (1994) NMR structure of the N-terminal SH3 domain of GRB2 and its complex with a proline-rich peptide from Sos. *Nat. Struct. Biol. 1*, 898−907.
(30) Terasawa, H., Kohda, D., Hatanaka, H., Tsuchiya, S., Ogura, K., Nagata, K., Ishii, S., Mandiyan, V., Ullrich, A., Schlessinger, J., et al. (1994) Structure of the N-terminal SH3 domain of GRB2 complexed with a peptide from the guanine nucleotide releasing factor Sos. *Nat. Struct. Biol. 1*, 891−897.
(31) Guruprasad, L., Dhanaraj, V., Timm, D., Blundell, T. L., Gout, I., and Waterfield, M. D. (1995) The crystal structure of the N-terminal SH3 domain of Grb2. *J. Mol. Biol. 248*, 856−866.
(32) McDonald, C. B., Seldeen, K. L., Deegan, B. J., and Farooq, A. (2009) SH3 Domains of Grb2 Adaptor Bind to PXpsiPXR Motifs Within the Sos1 Nucleotide Exchange Factor in a Discriminate Manner. *Biochemistry 48*, 4074−4085.
(33) McDonald, C. B., Seldeen, K. L., Deegan, B. J., and Farooq, A. (2008) Structural Basis of the Differential Binding of the SH3 Domains of Grb2 Adaptor to the Guanine Nucleotide Exchange Factor Sos1. *Arch. Biochem. Biophys. 479*, 52−62.
(34) McDonald, C. B., Seldeen, K. L., Deegan, B. J., Lewis, M. S., and Farooq, A. (2008) Grb2 adaptor undergoes conformational change upon dimerization. *Arch. Biochem. Biophys. 475*, 25−35.
(35) Gasteiger, E., Hoogland, C., Gattiker, A., Duvaud, S., Wilkins, M. R., Appel, R. D., and Bairoch, A. (2005) Protein Identification and Analysis Tools on the ExPASy Server. In *The Proteomics Protocols Handbook* (Walker, J. M., Ed.) pp 571−607, Humana Press, Totowa, NJ.
(36) Zimm, B. H. (1948) The Scattering of Light and the Radial Distribution Function of High Polymer Solutions. *J. Chem. Phys. 16*, 1093−1099.
(37) Wyatt, P. J. (1993) Light Scattering and the Absolute Characterization of Macromolecules. *Anal. Chim. Acta 272*, 1−40.
(38) Berne, B. J., and Pecora, R. (1976) *Dynamic Light Scattering*, Wiley, New York.
(39) Chu, B. (1991) *Laser Light Scattering: Basic Principles and Practice*, Academic Press, Boston.
(40) Koppel, D. E. (1972) Analysis of Macromolecular Polydispersity in Intensity Correlation Spectroscopy. *J. Chem. Phys. 57*, 4814−4820.
(41) Wiseman, T., Williston, S., Brandts, J. F., and Lin, L. N. (1989) Rapid measurement of binding constants and heats of binding using a new titration calorimeter. *Anal. Biochem. 179*, 131−137.
(42) Marti-Renom, M. A., Stuart, A. C., Fiser, A., Sanchez, R., Melo, F., and Sali, A. (2000) Comparative Protein Structure Modeling of Genes and Genomes. *Annu. Rev. Biophys. Biomol. Struct. 29*, 291−325.
(43) McDonald, C. B., Seldeen, K. L., Deegan, B. J., and Farooq, A. (2008) Structural basis of the differential binding of the SH3 domains of Grb2 adaptor to the guanine nucleotide exchange factor Sos1. *Arch. Biochem. Biophys. 479*, 52−62.
(44) Koradi, R., Billeter, M., and Wuthrich, K. (1996) MOLMOL: A program for display and analysis of macromolecular structures. *J. Mol. Graphics 14*, 51−55.
(45) Carson, M. (1991) Ribbons 2.0. *J. Appl. Crystallogr. 24*, 958−961.
(46) Van Der Spoel, D., Lindahl, E., Hess, B., Groenhof, G., Mark, A. E., and Berendsen, H. J. (2005) GROMACS: Fast, flexible, and free. *J. Comput. Chem. 26*, 1701−1718.
(47) Hess, B. (2008) GROMACS 4: Algorithms for Highly Efficient, Load-Balanced, and Scalable Molecular Simulation. *J. Chem. Theory Comput. 4*, 435−447.
(48) Jorgensen, W. L., and Tirado-Rives, J. (1988) The OPLS Force Field for Proteins: Energy Minimizations for Crystals of Cyclic Peptides and Crambin. *J. Am. Chem. Soc. 110*, 1657−1666.
(49) Kaminski, G. A., Friesner, R. A., Tirado-Rives, J., and Jorgensen, W. L. (2001) Evaluation and Reparametrization of the OPLS-AA Force Field for Proteins via Comparison with Accurate Quantum Chemical Calculations on Peptides. *J. Phys. Chem. B 105*, 6474−6487.
(50) Toukan, K., and Rahman, A. (1985) Molecular-dynamics study of atomic motions in water. *Phys. Rev. B 31*, 2643−2648.
(51) Berendsen, H. J. C., Grigera, J. R., and Straatsma, T. P. (1987) The Missing Term in Effective Pair Potentials. *J. Phys. Chem. 91*, 6269−6271.
(52) Darden, T. A., York, D., and Pedersen, L. (1993) Particle mesh Ewald: An N.log(N) method for Ewald sums in large systems. *J. Chem. Phys. 98*, 10089−10092.
(53) Hess, B., Bekker, H., Berendsen, H. J. C., and Fraaije, J. G. E. M. (1997) LINCS: A linear constraint solver for molecular simulations. *J. Comput. Chem. 18*, 1463−1472.
(54) Maignan, S., Guilloteau, J. P., Fromage, N., Arnoux, B., Becquart, J., and Ducruix, A. (1995) Crystal structure of the mammalian Grb2 adaptor. *Science 268*, 291−293.
(55) Dunker, A. K., Lawson, J. D., Brown, C. J., Williams, R. M., Romero, P., Oh, J. S., Oldfield, C. J., Campen, A. M., Ratliff, C. M., and Hipps, K. W. (2001) Intrinsically Disordered Protein. *J. Mol. Graphics Modell. 19*, 26−59.
(56) Dunker, A. K., Cortese, M. S., Romero, P., Iakoucheva, L. M., and Uversky, V. N. (2005) Flexible nets. The roles of intrinsic disorder in protein interaction networks. *FEBS J. 272*, 5129−5148.
(57) Liu, J., Perumal, N. B., Oldfield, C. J., Su, E. W., Uversky, V. N., and Dunker, A. K. (2006) Intrinsic disorder in transcription factors. *Biochemistry 45*, 6873−6888.
(58) Haynes, C., Oldfield, C. J., Ji, F., Klitgord, N., Cusick, M. E., Radivojac, P., Uversky, V. N., Vidal, M., and Iakoucheva, L. M. (2006) Intrinsic disorder is a common feature of hub proteins from four eukaryotic interactomes. *PLoS Comput. Biol. 2*, e100.
(59) Uversky, V. N. (2011) Intrinsically disordered proteins from A to Z. *Int. J. Biochem. Cell Biol. 43*, 1090−1103.
(60) Shimizu, K., Hirose, S., and Noguchi, T. (2007) POODLE-S: Web application for predicting protein disorder by using physicochemical features and reduced amino acid set of a position-specific scoring matrix. *Bioinformatics 23*, 2337−2338.
(61) Rabanal, F., Ludevid, M. D., Pons, M., and Giralt, E. (1993) CD of proline-rich polypeptides: Application to the study of the repetitive domain of maize glutelin-2. *Biopolymers 33*, 1019−1028.
(62) Kelly, S. M., Jess, T. J., and Price, N. C. (2005) How to study proteins by circular dichroism. *Biochim. Biophys. Acta 1751*, 119−139.
(63) Houtman, J. C., Yamaguchi, H., Barda-Saad, M., Braiman, A., Bowden, B., Appella, E., Schuck, P., and Samelson, L. E. (2006) Oligomerization of signaling complexes by the multipoint binding of GRB2 to both LAT and SOS1. *Nat. Struct. Mol. Biol. 13*, 798−805.